Revisiting weight-gain correlations for as-fabricated Zircaloy-4 cladding tubes during steam oxidation

Jean Desquines, Tatiana Taurines, Séverine Guilbert, Christian Duriez, Antoine Ambard

▶ **To cite this version:**

Jean Desquines, Tatiana Taurines, Séverine Guilbert, Christian Duriez, Antoine Ambard. Revisiting weight-gain correlations for as-fabricated Zircaloy-4 cladding tubes during steam oxidation. Journal of Nuclear Materials, 2022, 569, pp.153908. 10.1016/j.jnucmat.2022.153908 . irsn-03992948

HAL Id: irsn-03992948
https://irsn.hal.science/irsn-03992948

Submitted on 16 Feb 2023

HAL is a multi-disciplinary open access archive for the deposit and dissemination of scientific research documents, whether they are published or not. The documents may come from teaching and research institutions in France or abroad, or from public or private research centers.

L'archive ouverte pluridisciplinaire **HAL**, est destinée au dépôt et à la diffusion de documents scientifiques de niveau recherche, publiés ou non, émanant des établissements d'enseignement et de recherche français ou étrangers, des laboratoires publics ou privés.

Distributed under a Creative Commons Attribution - NonCommercial - NoDerivatives 4.0 International License

Revisiting weight-gain correlations for as-fabricated Zircaloy-4 cladding tubes during steam oxidation

Jean Desquines, Tatiana Taurines, Séverine Guilbert, Christian Duriez, Antoine Ambard

Abstract

During a loss of coolant accident, elevated temperatures and steam environment induce fuel cladding oxidation. During cladding high-temperature oxidation, the weight increase is considered as a material property when divided by the surface exposed to the environment, this is the so-called weight-gain. Many laboratories tested Zircaloy-4 specimens and used several approaches to determine weight-gain correlations. Two frequently used methods are weight measurements and metallographic measurements of scale thickness combined with diffusion simulations. Usually, assuming that weight-gain is controlled by diffusion processes, the correlations have a parabolic dependency to steam exposure duration. In the present study, a metallographic method relying on scale thickness measurements is proposed with few assumptions on the oxygen transport process in the oxide and α(O) layers. These two layers contain the main oxygen inventory. The local weight-gain is obtained by the integration of a simplified oxygen profile across the specimen thickness. The proposed method is compared to specimen weighing approach and leads to accurate predictions. The method was applied to five experimental campaigns performed in different laboratories combining more than 375 tests. A single non-parabolic weight-gain correlation covering a large temperature range (900 to 1500°C) is finally provided.

1 Introduction

The weight-gain can be defined as the mass change by area unit of the flat surface of a body exposed to an oxidizing environment. This is expected to represent a material property for a given oxidizing environment. Starting from this definition, the weight-gain is usually assessed measuring a specimen mass change divided by its surface exposed to the oxidizing environment.

Weight-gain is used to evaluate oxygen content in zirconium claddings and is also necessary to evaluate ECR (Equivalent Cladding Reacted) widely used to assess cladding embrittlement criteria in case of loss-of-coolant accident (LOCA) [BIL08, CAB15, BOU15, NAR20]. Usually, weight-gain is given as a correlation between various parameters of importance such as time at temperature, temperature, gaseous environment composition, etc.

The present paper proposes an improved correlation for weight-gain (wg) of Zircaloy-4 cladding tubes during steam oxidation at elevated temperature. The steam oxidation kinetics of cladding materials at elevated temperature is usually characterized by the specimen mass-increase, Δm, by surface units S exposed to the steam environment. It is usually adjusted as a power law increase with exposure duration to steam, $t\,(s)$, and also considered as a thermally activated parameter governed by an Arrhenius type dependency on temperature:

$$\left(\frac{\Delta m}{S}\right)^n = K_w . e^{-\frac{Q}{RT(K)}} t \quad (1)$$

Equation 1 indicates the importance of temperature in oxidation kinetics. Moreover, temperature evolution may be affected by an over-shoot (on as-received samples) or spatial heterogeneities. Temperature control and measurement are key parameters for oxidation kinetics studies.

There are currently many existing correlations that are not always fitting well together [BAK62, BAL76, GRA08, BAL76, CAT77, LEI83, LEI87, SCH03, LEM57, URB78, KAW78, NAG03, GRO10], as illustrated in Figure 1, with their validity range provided in Table 1. In Figure 1, most of the correlations set n=2 in eq. 1., thus assuming a simple controlled diffusion regime with a constant oxygen diffusivity over time, leading to the so-called parabolic regime [WAG33]. However, significant deviations from this simple situation have often been observed, specifically for the lower range of the temperature domain considered (T<1000°C). Values of the n exponent of up to 3 have been reported [NAG03, ZIN21]. Various reasons, likely strongly coupled, may explain the deviation from the parabolic regime: an increase over time (as the scale is growing) of the compressive stresses [GUE15], of the grain size (thus a decrease of the grain boundaries area) and/or of the monoclinic zirconia phase fraction [GUI19] will all result in a decrease of the oxygen mean diffusivity, leading to a n>2 exponent. Therefore, choice will be made for the present paper to adjust the analysed data with a variable n exponent power law.

The methods used to determine the weight-gain can be categorized depending on measurement scale: either specimen scale or local scale (cladding thickness at a given position).

Among global weight-gain measurements one can find:

- hydrogen release measurement, assuming no hydrogen pickup during high-temperature oxidation [LEM57, BAK62, URB78],

- specimen weighing before and after high temperature oxidation [URB78, KAW78, NAG03, GRO10, GUI10, GUI21].

Weight measurements before and after the test are extremely accurate but are sometimes affected by specimen edge effects, which must be carefully corrected. The temperature influence on specimen weight is also affected by spatial heterogeneities of its temperature. This is noticeably the situation when studying long rodlets after semi-integral tests.

The main local methods are based on:

- oxide and oxygen stabilized α(O) scale measurement and diffusion modeling [BAL76, CAT77, LEI87, LEI87, SCH03],

- micro-hardness profiles used to determine oxygen profiles across the cladding relying on oxygen hardening and calibration of the method [POR05],

- detailed metallurgical methods, such as neutron activation analysis [BAL76] or Castaing microprobe [POR05, BRA11, LES11, DUR11], which can generate oxygen profile but have not been used to generate weight-gain correlation to our knowledge.

Deriving weight-gain from oxygen affected scale thickness measurements is usually performed along with diffusion simulations [CAT77, CHU80]. This approach leads quite systematically to a parabolic weight-gain kinetics whereas some experimental global measurements follow a non-parabolic kinetics, in particular at temperatures lower than 1000°C [NAG03]. Using welded thermocouples, the temperature was measured at the same axial position as for the scale thickness measurement using

welded thermocouples leading to an accurate evaluation of weight-gain temperature dependency at an azimuth away from welding location.

Reference	Material	Method used	Temperature range (°C)
Baker-Just [BAK62]	Zr	H_2 release	1000 - 1852
Klepfer [BAL76, GRA08]	Zr-4	Not available in the mentioned references	890-1577
Ballinger [BAL76]	Zr-4	Local : simplified [O] (r) profile + NAA	871-1482
Cathcart-Pawel (CP) [CAT77]	Zr-4	Local : simplified [O](r) profile	1000-1500
Leistikov [LEI83, LEI87], [SCH03]	Zr-4	Local : simplified [O](r) profile	900-1500
Lemmon [LEM57], [GRA08]	Zr-2&Zr	H_2 release	1000 - 1400
Urbanic [URB78]	Zr-2&4	weighing and H_2 release	1050-1580
Kawazaki [KAW78]	Zr-4	weighing	950-1330
Nagase [NAG03]	Zr-4	weighing	500-1300
Grosse [GRO10]	Zr-4	weighing	800-950 & 1000-1400

Table 1: Some key publications providing parabolic weight-gain correlations (i.e. n=2 in eq.1).

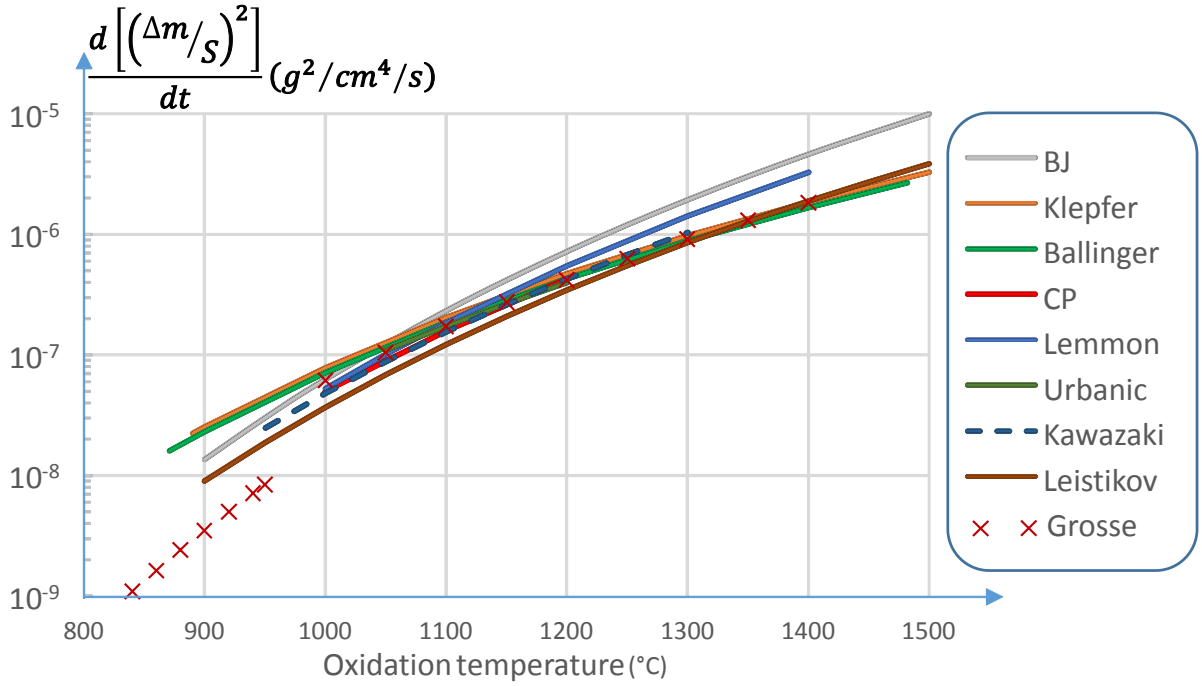

Figure 1: Comparison of some of the main weight-gain correlations from literature.

In this work, a new method is developed to determine the Zy-4 weight-gain during steam oxidation based on metallographic data from tests performed at IRSN. This method is then validated on a wide set of experimental programs from literature. Finally, a novel non parabolic weight-gain correlation is established covering a large range of temperatures (900-1500°C).

2 Metallography-based model

2.1 Oxygen profile, experiment and schematic

After steam oxidation at elevated temperature, the oxygen profile can be determined quantitatively in the metallic part of the specimen using a Castaing microprobe as illustrated in Figure 2. First, at surface an oxide layer develops. The oxygen profile across the oxide layer is not accurately known. Unfortunately, oxygen profile measurement in oxide scales is complex due to the open porosity and electron accumulation in the oxide (ZrO_2 is a non-conductive ceramic).

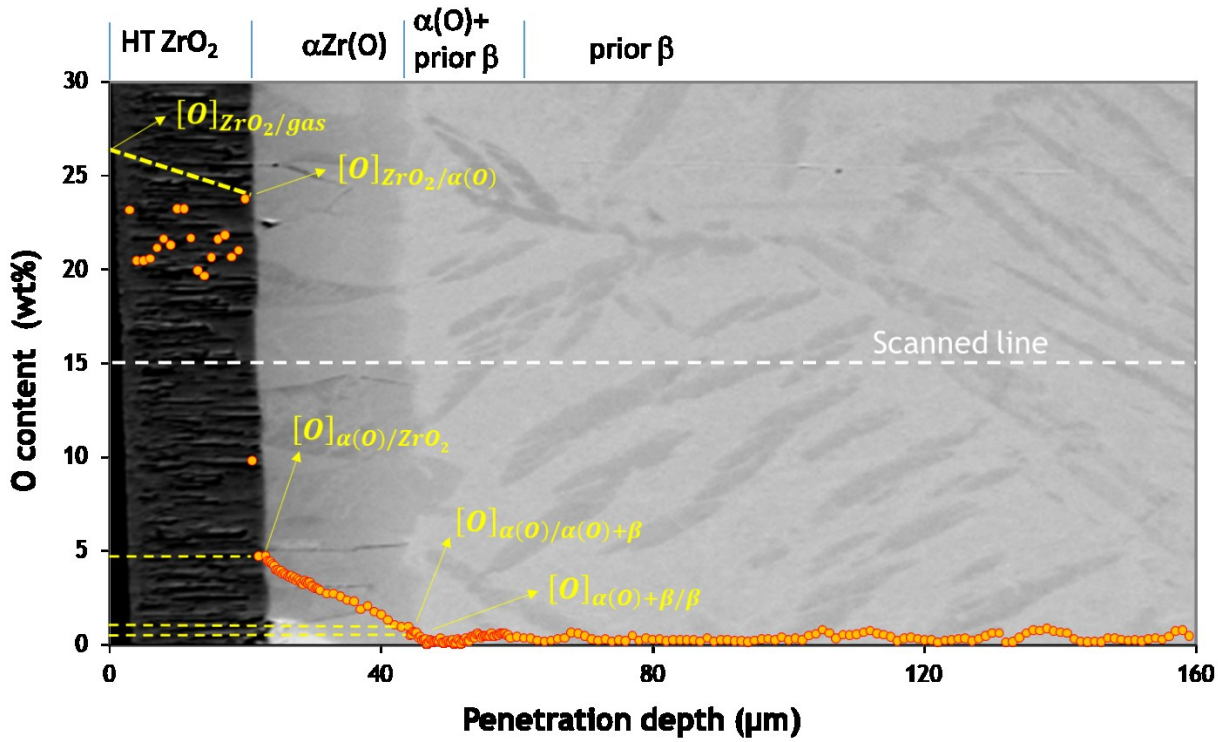

Figure 2: Typical oxygen distribution after high temperature steam oxidation of a specimen measured using a Castaing microprobe.

However, assuming usual process for zirconium alloy anionic-oxidation, oxygen vacancies diffuse from oxide-metal interface towards oxide surface in contact with gaseous environment. Oxygen from gaseous environment is captured into a vacancy and transported towards the oxide metal interface. A monotonously decreasing oxygen distribution is generally considered with a maximum at the gaseous oxide interface and a rather lower oxygen content at the oxide -metal interface [MA08].

Steep decreases in oxygen concentration in the metal at the oxide-metal interface and to a lesser extent locally at the α(O)/β interface are also expected. These two steep changes can be interpreted as discontinuities in the oxygen content profile.

This continuous oxygen concentration profile can be schematized as illustrated in Figure 2:

- a linear oxygen profile in the oxide layer, varying between $[O]_{ZrO_2/gas}$ and $[O]_{ZrO_2/\alpha(O)}$,

- a linear profile in the α(O) layer, varying between $[O]_{\alpha(O)/ZrO_2}$ and $[O]_{\alpha(O)/\alpha(O)+\beta}$,

- a constant oxygen content in the ex-β phase corresponding to the average oxygen content $(\overline{[O]}_{ex-\beta})$.

The oxygen profile across the cladding can then be redrawn as illustrated in Figure 3 using the proposed simplifications.

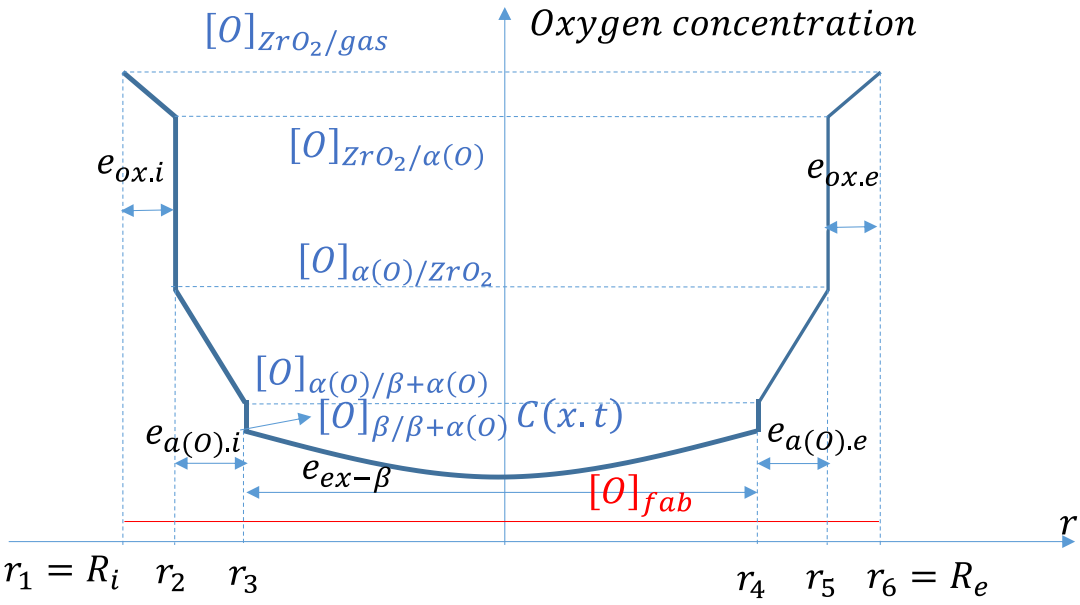

Figure 3: Simplified oxygen profile for two-sided oxidation across the cladding thickness.

2.2 Simplified oxygen profile and integration

The weight change of the specimen can be described by the following equation

$$\Delta m = \int_{\Omega_{ox}} \widetilde{[O]}(M_{ox}) \rho_M\left(\widetilde{[O]}(M_{ox})\right) d\Omega_{ox} - \int_{\Omega} [O]_{fab} . \rho_M([O]_{fab}) d\Omega \qquad (2)$$

Where $[O]_{fab}$ is the as-fabricated oxygen content (in wt%),

$\widetilde{[O]}(M_{ox})$ is the oxygen concentration in the as-oxidized, Ω_{ox} volume,

Ω is the volume of the considered specimen before high temperature oxidation,

Ω_{ox} is the volume of the specimen after high temperature oxidation,

The material densities at room temperatures are taken [ATI15, MAT93]:

$$\rho_M([O]) = \begin{cases} \rho_{Zr-4} = 6.55 \frac{g}{cm^3} in\ the\ metal \\ \rho_{ZrO_2} = 5.82 \frac{g}{cm^3} in\ the\ oxide \end{cases} \qquad (3)$$

Variations in the densities because of varying oxygen content are neglected.

We consider a plane section in a cylindrical or tubular specimen containing the symmetry axis of the specimen. The specimen height is H and its as-received surface exposed to oxidizing environment is S_{ox}. The oxygen concentration changes continuously (except for some discontinuous phase boundaries). It can be discretized in the radial direction $(r_i)_{i=1,\dots,n}$ after oxidation: $([O]_i)_{i=1,\dots,n}$. Each domain, as illustrated in Figure 4, has a constant material density $(\rho_{M,i})_{i=1,\dots,n}$. Following this discretization, the weight-gain can be analytically evaluated by:

$$wg = \frac{2.\pi.H}{S_{ox}} \left[\sum_{i=1}^{n-1} \rho_{M,i} \frac{(r_{i+1} - r_i)}{6} \{[O]_{i+1}(2r_{i+1} + r_i) + [O]_i(2r_i + r_{i+1})\} - \frac{[O]_{fab}}{2} . \rho_{Zr} . \left(R_{e,0}^2 - R_{i,0}^2\right) \right] \qquad (4)$$

$R_i = r_1$ and $R_e = r_n$ are respectively the inner and outer radius of the oxidized specimen and $R_{i,0}$ and $R_{e,0}$ as-fabricated inner and outer radius.

Neglecting the slight increase of S_{ox} induced by oxidation, the pre-factor can be simplified into:

$$\frac{2.\pi.H}{S_{ox}} = \begin{cases} \frac{1}{R_{e,0}} \; for\ single\ side\ outer\ diameter\ oxidation \\ \frac{1}{R_{e,0}+R_{i,0}} \; for\ two-side\ oxidation \end{cases}$$

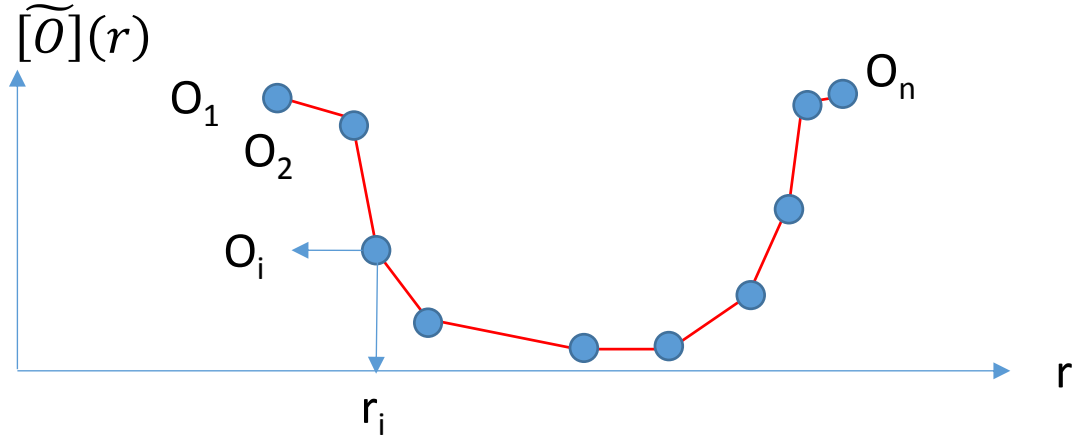

Figure 4: Discretized oxygen profile across a tubular specimen (2 sides oxidation).

In case of a discontinuity in the oxygen profile:

$$[O]_i = \begin{cases} [O]_i^+ \; for\ r > r_i \\ [O]_i^- \; for\ r < r_i \end{cases}$$

The discretization remains unchanged if the discontinuity radius r_i is integrated into the subdivision of the integration domain:

$$wg = \frac{2.\pi.H}{S_{ox}} \left[\sum_{i=1}^{n-1} \rho_{M,i} \frac{(r_{i+1}-r_i)}{6} \{ [O]_{i+1}^- (2r_{i+1} + r_i) + [O]_i^+ (2r_i + r_{i+1}) \} - \frac{[O]_{fab}}{2} . \rho_{Zr} . \left(R_{e,0}^2 - R_{i,0}^2 \right) \right] \quad (5)$$

This last equation is useful at the oxide-metal and at the α/β interface where there is a discontinuity in the oxygen profile as observed in Zircaloy-4.

The number of discretization points is fixed using the simplified oxygen profile illustrated in Figure 3 and detailed in Table 2.

Radius	r_1	r_2	r_3	r_4	r_5	r_6
position	inner radius	α(O)/ZrO_2 inner interface	α(O)/ex β inner interface	α(O)/ex β outer interface	α(O)/ZrO_2 outer interface	outer surface

Table 2: Radial discretization points.

The Pilling-Bedworth (PB) ratio describes the volume increase when transforming a metal into oxide. For zirconium oxidation into zirconia the PB ratio is 1.56. High temperature oxidation of a cladding

consequently induces an increase in cladding diameter mainly resulting from the metal to oxide transformation volume change. To assess the modified radius after steam oxidation:

$$r_6 = R_e = R_{e,0} + \frac{e_{ox,e}+e_{ox,i}}{PB} \quad (6)$$

$$r_1 = R_i = R_e - e_{ox,e} - e_{ox,i} - e_{\alpha(O),e} - e_{\alpha(O),i} - e_{ex-\beta} \quad (7)$$

$$r_2 = R_e - e_{ox,e} - e_{\alpha(O),e} - e_{\alpha(O),i} - e_{ex-\beta} \quad (8)$$

$$r_3 = R_e - e_{ox,e} - e_{\alpha(O),e} - e_{ex-\beta} \quad (9)$$

$$r_4 = R_e - e_{ox,e} - e_{\alpha(O),e} \quad (10)$$

$$r_5 = R_e - e_{ox,e} \quad (11)$$

Using this radius discretization and equation (5), the weight-gain can be derived from metallography for two-sided and one-sided steam oxidation.

Finally, weight-gain comes from the oxygen in the oxide (usually about 75 wt%), in the α(O) (usually about 20 wt%) phase and in the ex-β phase. The above described three contributions are ordered by decreasing contribution to the specimen weight-gain. The ex-β phase contribution to the weight-gain is rather small (usually less than 5 wt%) and low accuracy evaluation is sufficient. The contribution of the oxide layer is clearly the most important one and must be determined accurately. The determination of α(O) contribution is more challenging because it is rather difficult to measure accurately the thickness of this layer. The proposed linearization in the α-phase appears reasonable. The linear distribution within the oxide is not validated by any existing experience. But this assumption is rather consistent with existing simulations assuming oxygen diffusion within the oxide layer [MA08, DUR11, MAZ13, BAR19, KIM21]. Diffusion usually leads to a convex evolution of the oxygen profile. However, some detailed modeling of the chemical potential tends to show that there might be an oxygen content profile concavity in the α(O) layer [BAR19] and this curvature was sometimes observed when performing microprobe oxygen profile measurements [BRA08, DUR11]. Despite this, a linear approximation in the α(O) oxygen content profile is assumed which significantly simplifies the data analysis.

The benefits of the proposed approach relies on several factors:

- the proposed wg is close to a direct measurement in a local region based on a metallography relying on a limited number of assumptions,

- the specimen edge effects don't need to be corrected and temperature heterogeneities along the specimen cannot affect the proposed weight-gain measurement if the temperature at the metallographic cut position has been checked,

- no assumption is made for the oxide layer growth kinetics. Consequently, non-parabolic growth rate can be handled using the proposed approach.

The main weakness of the proposed approach relies on the fact that the formation of α(O) inclusions in the ex-β region is not described. Consequently, the contribution of α(O) inclusions on the weight-gain is not taken into account and for very long steam exposures at elevated temperature the actual wg is expected to exceed the calculated value.

The oxidized surface curvature or cutted-edges might affect the accuracy of the measured specimen weight-gain. Tube specimens usually exhibit slightly thinner oxide scales at internal surface than external one suggesting a possible slight difference in oxidation kinetics for flat or tubular geometries.

2.3 Interface oxygen concentrations

The Zr-O phase diagram has been studied by many authors. Domagala and Pherson [DOM54] phase diagram for Zr-O showed an important trend about zirconia stability. Sub-stoichiometric zirconia is considered to be the stable composition at the α(O)-ZrO_2 boundary. Nevertheless, there is a need for improved experimental stoichiometry characterization of the zirconia at the oxide-metal interface to determine an accurate oxygen concentration. Complementary studies by Gebhardt [GEB61] and Ruh [RUH1967, GOS15] indicate that three allotropic forms of zirconia coexist for oxygen contents over 22 wt% depending on the temperature and material composition:

- monoclinic zirconia below approximately 1000°C,

- tetragonal zirconia above this temperature,

- cubic zirconia forms above 1500°C, appearing interspersed with metallic needles in metallographs [GEB61, RUH66]

Ma [MA08] revisited the domains of stability of the various allotropic forms of zirconia and better interpreted the past experiments [DOM76, GEB61, RUH66]. The phase diagram proposed by Ma is superimposed with the Domagala phase diagram in Figure 5.

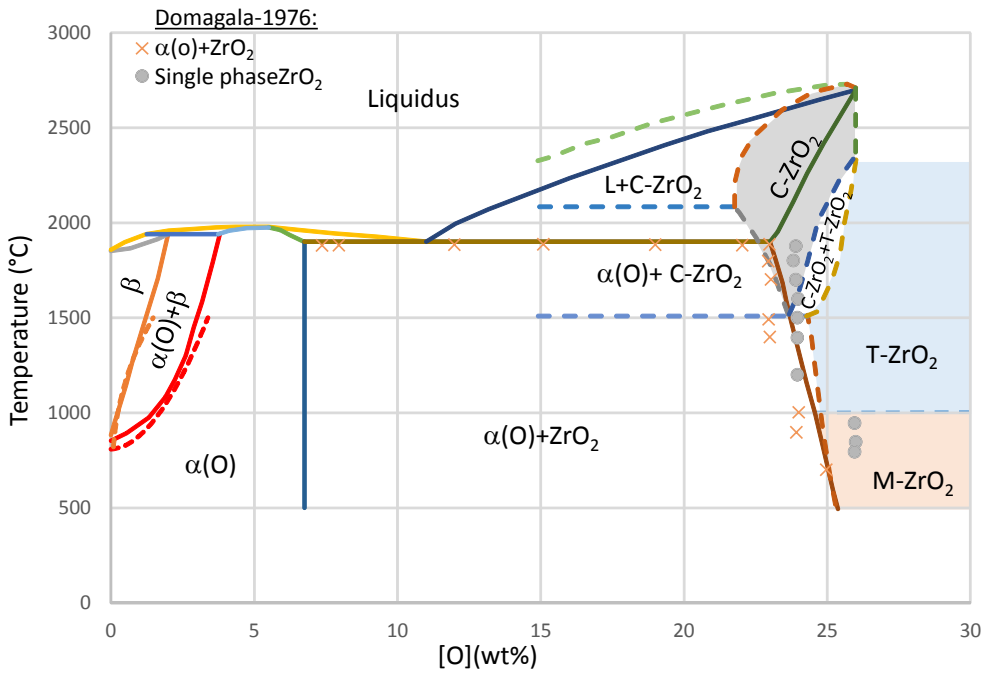

Figure 5: Zr-O phase diagram ([DOM76] solid lines – cross marks correspond to specimen containing a(O) & ZrO_2 mixtures and grey dots to specimen containing ZrO_2 as single phase, [MA2008] dashed lines above 15 wt% [O], [CHU79] doted lines below 3 wt% [O])

Below 1500°C, only monoclinic and tetragonal zirconia has to be considered. In the following, only temperatures below 1500°C are considered. The phase transformation domains for zirconia are also known to be influenced by hydrostatic stresses and grain size [GOS15, BUD93]. Consequently, the provided oxygen concentration must be considered as indicative values.

At oxygen contents below 3 wt%, a pseudo-binary phase diagram was established experimentally by Chung and Kassner [CHUN79] identifying α(O), β and α(O)+β domains of stability with very good accuracy for Zircaloy-4. This diagram confirms that the tin is an β-Zr stabilizer slightly decreasing the $\alpha/\alpha+\beta$ transformation temperature as illustrated in Figure 5.

There is some limited hydrogen uptake during high temperature steam oxidation. Consequently, the influence of hydrogen content will be discussed in the following.

There is few controversies on oxygen content at the gas/zirconia layer interface. Cathcart & Pawel proposed to consider stoichiometric zirconia with $[O]_{ZrO_2/gas} = 25.96\ wt\%$. There is usually negligible hydrogen content in the zirconia, consequently the boundary concentrations in this layer are not affected by hydrogen content in the cladding specimen.

Figure 5 shows that the oxygen content in the zirconia at the zirconia/α(O) layer interface is comprised between 23 and 25 wt% in the 700-1500°C range and the zirconia formed at the interface is clearly sub stoichiometric as already discussed in the previous section. However, the contribution of the uncertainty on this interfacial concentration will result in any case in an uncertainty lower than 4 to 8% without further refinements. With some consistency with the Domagala phase diagram, Cathcart & Pawel [CAT77] used $[O]_{ZrO_2/\alpha(O)}(wt\%) = 26 - \frac{T(K)}{776}$. But as shown in Figure 5, the experiments supporting this limit are scarce and there is limited accuracy on this concentration. The correlation to be used in this study will be refined in an upcoming section.

In the present study, the concentration in the α(O) at the α(O)/ZrO_2 interface is taken equal to $[O]_{\alpha(O)/ZrO_2} = 7\ wt\%$ as recommended by Cathcart and Pawel [CAT77] whatever the oxidation temperature or hydrogen content are.

The concentration in the α(O) layer at the α(O)/ex-β interface is extracted from Chung experiments [CHU79] who experimentally updated the boundary composition specifically testing Zircaloy-4 at different temperatures T(K): $[O]_{\alpha(O)/\beta+\alpha(O)}(wt\%) = 100.e^{-2.28+0.0535ln(T(K)-1083)}$. Torres [TOR17] has shown that average hydrogen contents up to 400 wppm had limited influence on this solubility limit, and Guilbert [GUI16] extended this conclusion for temperatures ranging between 1000 and 1200°C. At higher hydrogen contents, an influence of hydrogen content is expected as shown by Guilbert [GUI16].

The model given by Chung [CHU79] is also used for the boundary concentration in the ex-β at the ex-β/α(O) interface: $[O]_{\beta/\beta+\alpha(O)}(wt\%) = 100.e^{-5.02+\frac{8220}{T(K)}}$. Similarly, Torres [TOR17] and Guilbert [GUI16] contributed to show that this solubility limit is not significantly influenced by hydrogen content up to 1000 wppm.

2.4 Oxygen content in the ex-β phase

The oxygen transport in the ex-β phase layer is controlled by diffusion, consequently in this scale the diffusion is modeled to provide satisfactory extrapolations for short duration exposure since the $\alpha(O) + \beta$ is not considered. In the following, a Crank [CRA56] analytical solution is used. The reference situation is illustrated in Figure 4. The solution is established for the study of the gas charging of a 2l thick plate with a constant gas concentration at the edge s of the plate. Theoretically, this solution cannot be used to describe a problem with moving α-β interfaces during the diffusion process. However, this approximation is accurate for short term oxidation (small movement of the interface) and the contribution of this phase to the weight-gain becomes negligible for long term exposure thus this approximation appears as a good compromise to determine the specimen weight-gain resulting from the β phase. In the following, the oxygen diffusion in the β phase between α/β interfaces (double side oxidation) is considered. Both interfaces are located at $\pm l$.

The time and space distribution of solute between -l and +l is given by the following series:

$$\frac{c(x,t)-c_0}{c_s-c_0} = 1 - \frac{4}{\pi}\sum_{n\geq 0}\left[\frac{(-1)^n}{2n+1} e^{-\frac{D(2n+1)^2\pi^2 t}{4l^2}} . cos\left\{\frac{(2n+1)\pi x}{2l}\right\}\right]$$

Where c_0 is the initial solute concentration and c_s the solubility limit.

The average solute concentration, $\bar{c}$, in the solid solution at each time can be determined using the above-mentioned equation: $\bar{c} = \frac{1}{2l}\int_{-l}^{+l} C(x,t)dx$:

$$\frac{\bar{c}-c_0}{c_s-c_0} = 1 - 8\sum_{n\geq 0}\left[\frac{1}{\pi^2(2n+1)} e^{-\frac{D(2n+1)^2\pi^2 t}{4l^2}}\right]$$

The average content in the solid solution corresponds to the average content in the entire specimen. A simplified but very accurate solution is as follows:

$\frac{\bar{C}-C_0}{C_s-C_0} = Min\left[4\sqrt{\frac{\omega}{\pi}}; 1 - \frac{8}{\pi^2}\left\{e^{-\pi^2\omega} + \frac{e^{-9\pi^2\omega}}{9} + \frac{e^{-25\pi^2\omega}}{25}\right\}\right]$ (error <3.10^{-5}%)

$\omega = \frac{D.t}{(2l)^2}$ is a normalized time parameter.

For two-sided oxidation during a LOCA, the ω parameter is $\omega = \frac{D_\beta.t}{(e_{ex-\beta})^2}$ and for one-sided oxidation $\omega = \frac{D_\beta.t}{(2e_{ex-\beta})^2}$.

D_β: is the diffusion coefficient of oxygen in the β-phase of Zircaloy-4.

A correlation from Perkins [PER77] is used in the following: $D_\beta(cm^2/s) = 0.0301.e^{-\frac{2880}{1,987.T(K)}}$.

And the average concentration of oxygen in the ex-β phase is then:

$$\overline{[O]}_{ex-\beta} = [O]_{fab} + \left([O]_{\alpha(O)/\beta+\alpha(O)} - [O]_{fab}\right) Min\left[4\sqrt{\frac{\omega}{\pi}}; 1 - \frac{8}{\pi^2}\left\{e^{-\pi^2\omega} + \frac{e^{-9\pi^2\omega}}{9} + \frac{e^{-25\pi^2\omega}}{25}\right\}\right] \quad (11)$$

The ex-β layer thickness appearing in ω parameter is obtained from measurements by subtracting α(O) and zirconia layers thickness measured using metallographs from the oxidized cladding specimen total thickness (difference between r3 and r4, see equations 10 and 9).

The oxygen content in the ex-β phase is assumed to be constant and following equation 11. The assumption of a constant oxygen concentration across the prior-beta-layer is inconsistent with Figure 3 although this is unlikely to have any numerical significance because of the way the average is calculated.

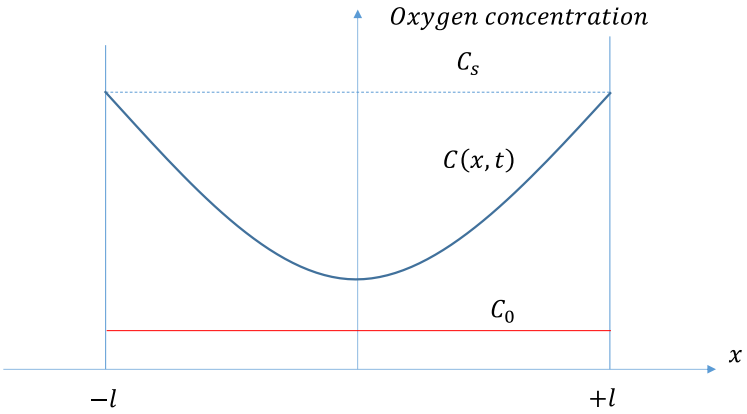

Figure 6: Space and time distribution of the solute for an infinite set of planar precipitates in an infinite media [CRA56].

2.5 Main datasets and validation of the method

A large set of steam oxidation experiments from five different bibliographical sources has been selected as summarized in Table 3. Some of them provide characterization of oxidation scale thicknesses (α(O) and ZrO_2) and other provide weight-gains based on specimen weighing before and after the test. Authors have not been able to fully reconstruct the Leistikov data and there is a possibility that some of the specimens were both characterized by metallography and weighing. Many specimens from an IRSN program have been characterized both by metallography and weighing. It is thus decided to calibrate the metallographic weight-gain measurement method based on these measurements.

Authors	Temperature range (°C)	Scale thickness available	wg form weighing available
Cathcart & Pawel [CAT77]	900-1500	yes	no
Sawarn [SAW16]	900-1200	yes	no
IRSN (Table 4)	900-1200	yes	yes

Leistikov [LEI83, LEI87], [SCH03]	650-1300	yes	no
Nagase [NAG03]	650-1300	no	yes

Table 3: The five experimental programs supporting the wg characterization in this study.

IRSN has been running experimental programs to characterize cladding material oxidation conditions for a long period. The testing protocols and some results are described in references [GUI10, GUI16B, GUI21]. Tests for which both a characterization of scale thicknesses and weight-gain deriving from weight measurements are available are listed in Table 4. Most of the tests are two-sided oxidations. Inner and outer oxidation layers are characterized independently using optical microscopy for most of the tests. A few steam oxidation tests are performed at 1200°C using sealed end plugs leading to one-sided oxidation. For some of the tests, the metallography is not sufficiently contrasted to measure α(O) layer thicknesses, in this case eddy current measurements combined with zirconia layer measurements are used to assess the oxygen stabilized α layer thickness [DES21]. In this situation, the α(O) layer thickness is assumed to be the same at inner and outer surfaces. This data set is used to calibrate as accurately as possible the oxygen concentration in the zirconia layer at the α(O) interface, $[O]_{ZrO_2/\alpha(O)}(wt\%)$. Indeed, this is the only lacking parameter to determine the metallography-based weight-gain.

Steam oxidation conditions		**e ZRO2 thickness**		**α(O) thickness**		**weighing**
Temperature	**duration**	**outer surface**	**inner surface**	**outer surface**	**inner surface**	**Measured wg**
(°C)	(s)	(µm)		(µm)		(g/cm^2)
900	600	9.4	9.1	16.7	16.3	0.00172
	1200	12.4	11	*16.5*	*16.5*	0.00238
	1800	15.2	13.5	17.2	16.8	0.00309
	3000	17.7	14.7	41.4	41.6	0.00319
	4500	17.5	15.5	51.7	50.8	0.00411
	6000	19.8	17.5	34.5	35.2	0.00435
		19.6	16.9	33.8	34.6	0.00440
		19.9	17.1	32.2	32.6	0.00448
1000	300	18.1	16.8	*18*	*18*	0.00337
		19	16.9	*15.8*	*15.8*	0.00335
	900	34.3	31.4	23.6	23.8	0.00633
	1500	37.8	33.2	*35.4*	*35.4*	0.00691
	1800	46.4	43.2	34.3	33.6	0.00862
		43.3	37.4	*40*	*40*	0.00788
		40.4	39.1	*46.8*	*46.8*	0.00807
	2400	47	44.2	*54.1*	*54.1*	0.00964
	3600	52	47.8	*68.5*	*68.5*	0.01098
1100	600	47.3	44.2	56.9	53.5	0.00876
	900	59.6	55.5	70.4	69.7	0.01121

1200	200	53.8	52.3	54.3	53	0.00965
	300	52.3	48.4	71.5	70.3	0.01022
	465	68.9	65.6	93.2	91.4	0.01394
		67.4	64.9	89.8	89.1	0.01344
		68.1	64.3	90.2	90.9	0.01351
		70.0	67.5	93.3	91.5	0.01399
		66.3	63.7	88.2	87.5	0.01348
		67.3	64.4	89.3	88.6	0.01341
		62.0	0.0	86.3	0	0.01288
		62.3	0.0	84.5	0	0.01259
		64.8	0.0	90.9	0	0.01342
	600	**89.3***	**89.3***	**88.4***	**85.1***	**0.01603***
		70.6	66.4	92.2	91	0.01348
	900	92.6	89	133.9	125.8	0.01846
		84.9	79.9	113.8	116.3	0.01666
	1860	121.2*	0.0	167.8*	0	0.02737*
		124.2	0.0	174.4	0	0.02493
		126.1	0.0	179.1	0	0.02496

Table 4: IRSN steam oxidation experiments with simultaneous wg measurement by weighing and metallographic characterization of the various scale thickness – Italic: eddy current measurement for $e_{\alpha(O)}$, *: some doubt on this value.

A linear dependence of the $[O]_{ZrO_2/\alpha(O)}$ concentrations with temperature is considered. Finally, the best fit of the IRSN weighing measurements with metallographic calculated weight-gains is obtained for the following correlation: $[O]_{ZrO_2/\alpha(O)}(wt\%)$: $[O]_{ZrO_2/\alpha(O)} = 25.3 - \frac{T(K)}{531}\ wt\%$. This correlation will be used in the rest of the study. Two of the test results are affected by uncertainty, probably resulting from a lack of accuracy in oxidation temperature assessment. Other results are in good adequacy for all temperatures comprised between 900 and 1200°C and a 5.5% standard deviation is obtained comparing the two estimates of weight-gain, which appears acceptable.

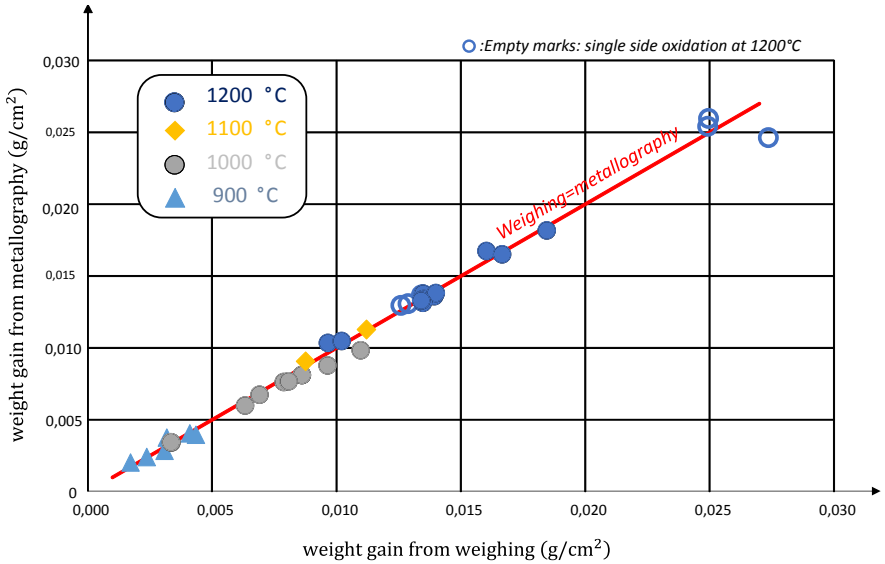

Figure 7: Comparison between weight-gain from weighing and from metallography full-marks correspond to two-sided oxidation and empty mark to one-sided oxidation.

3 Novel weight-gain correlation

The entire set of boundary layers concentrations is then used to determine the metallography- based weight-gain of two main testing campaigns for which authors also evaluated the weight-gain using diffusion modeling:

- Cathcart-Pawel test results [CAT77].

- Leistikov test results [LEI83. LEI87, SCH03].

The comparison between Cathcart & Pawel and Leistikov results are illustrated in Figure 8 showing that the present study leads to weight-gains consistent with Leistikov data, but rather higher than Cathcart & Pawel assessment. This slight deviation is observed for all tested conditions. This method can then be used with a reasonable confidence to jointly analyze the results from the various experimental programs listed in Table 3.

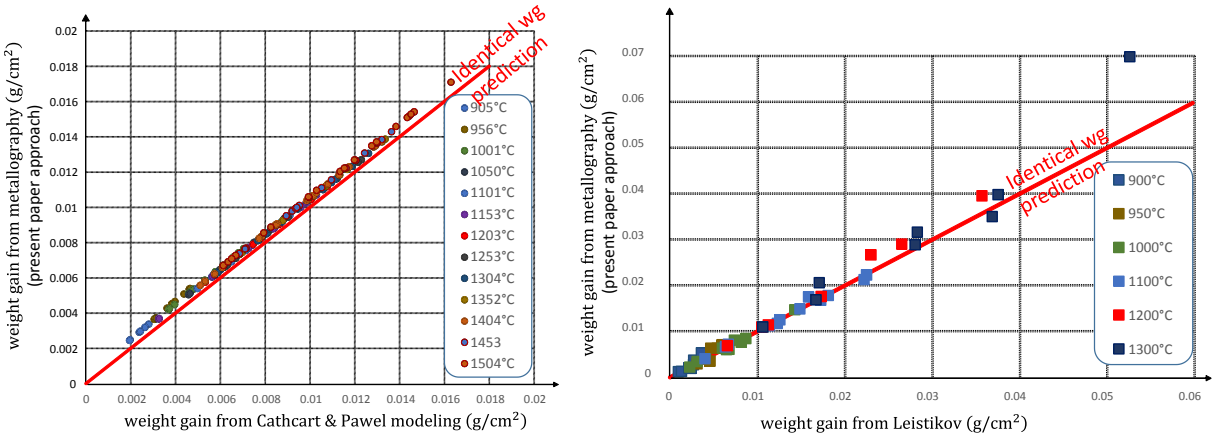

Figure 8: Comparison between present study weight-gains and values derived by: a) Cathcart & Pawel and b) Leistikov.

The obtained weight-gains are plotted in Figure 9 with different symbols associated to each bibliographical source and marks color depending on the temperature. The kinetics exponent, n, of the model is plotted and compared to the results of Nagase [NAG03] in Figure 10. The calculated values lead to slightly higher kinetics exponents than the ones proposed by Nagase in its validity range. It clearly appears in Figure 9, that the various experimental programs lead to rather consistent weight-gains except between 900 and 1000°C. It is frequently suspected that the monoclinic to tetragonal phase transformation of zirconia at 1000°C is partly responsible for the oxidation kinetics change and result scattering. In this temperature range, the Cathcart-Pawel and Leistikov oxidation kinetics are rather faster than the results from more recent programs. This might be the result of a metallurgical change such as a higher tin content for past alloys or differences in the manufacturing process. Therefore Cathcart-Pawel and Leistikov data at 900°C and 950°C were not considered to establish the correlation. For all other temperatures, all the data are taken into account to determine a weight-gain correlation covering the entire temperature range between 900 and 1500°C. A

quadratic error minimization procedure is applied to determine a simple shape function describing as accurately as possible this data set. The time dependency of this law is not parabolic, as suggested by Nagase [NAG03] and there is an acceleration of the oxidation kinetics above 1224°C appearing in the correlation, which is also consistent with Grosse results [GRO10]. Extrapolation below 900°C is not recommended since, consistently with [NAG03], a cubic kinetics (n=3) is observed. The proposed correlation is plotted and compared to the data in Figure 9. The accuracy of the proposed correlation is compared to experimental measurements and to Cathcart-Pawel correlation prediction in and out of its applicability range in Figure 10. The predictions are in rather good agreement with measured weight-gains except when using the Cathcart-Pawel correlation out of its validity range at 900 and 950°C. There are some underpredictions associated with oxidation times above 1000s at 1000°C. The optimization also provides the standard deviation at each temperature range of the estimated weight-gain assuming a log-normal distribution. The results are gathered in Table 5 and confirm a strong increase of the data scattering at 900, 950 and 1000°C. At 1000°C and above the scattering decreases with temperature increase. The proposed correlation leads systematically to slightly lower uncertainty than the one derived from Cathcart-Pawel correlation.

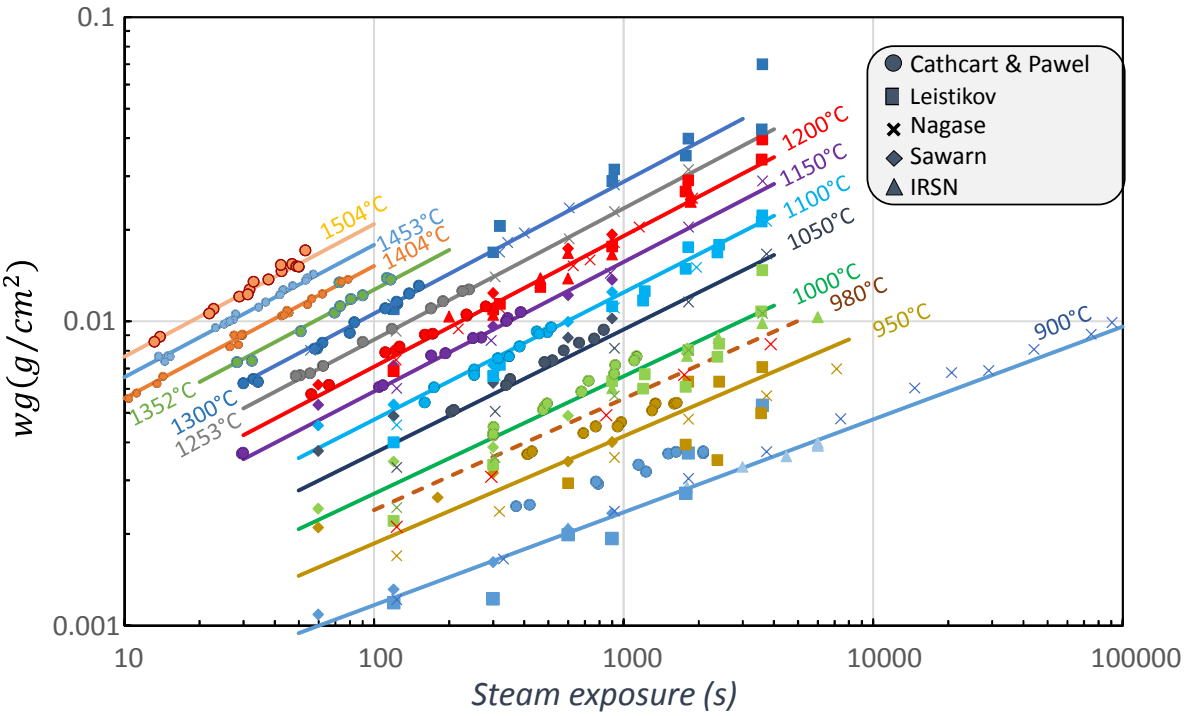

Figure 9: Five experimental sources and proposed weight-gain correlation calculated using the metallographic results

$$wg(g/cm^2) = 0.1207.\, e^{-\frac{7092}{T(K)}}\{1 + Max[9.33.10^{-4}(T(K) - 1497); 0]\}.\,[t(s)]^{\frac{1}{n}} \qquad (12)$$

$$n = 2.30 + 1.66.\, e^{-\frac{T(K)-1129}{83}} \qquad (13)$$

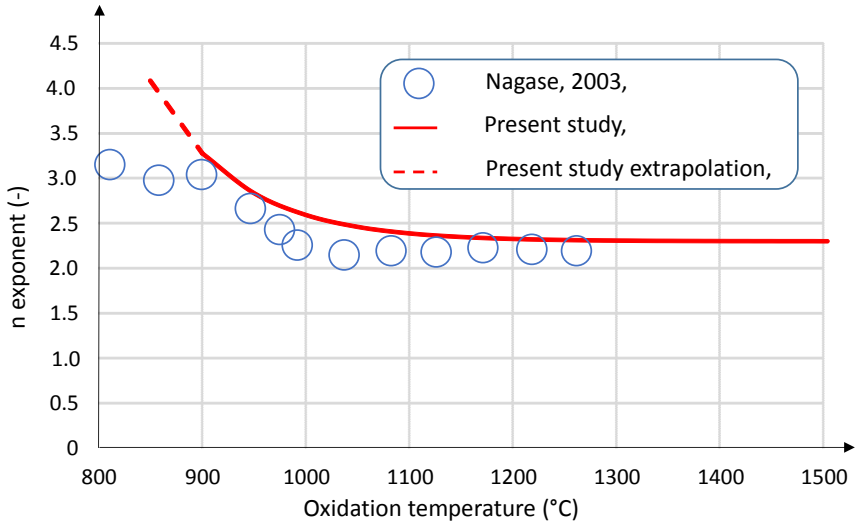

Figure 10: Evolution of kinetic exponent n with oxidation temperature.

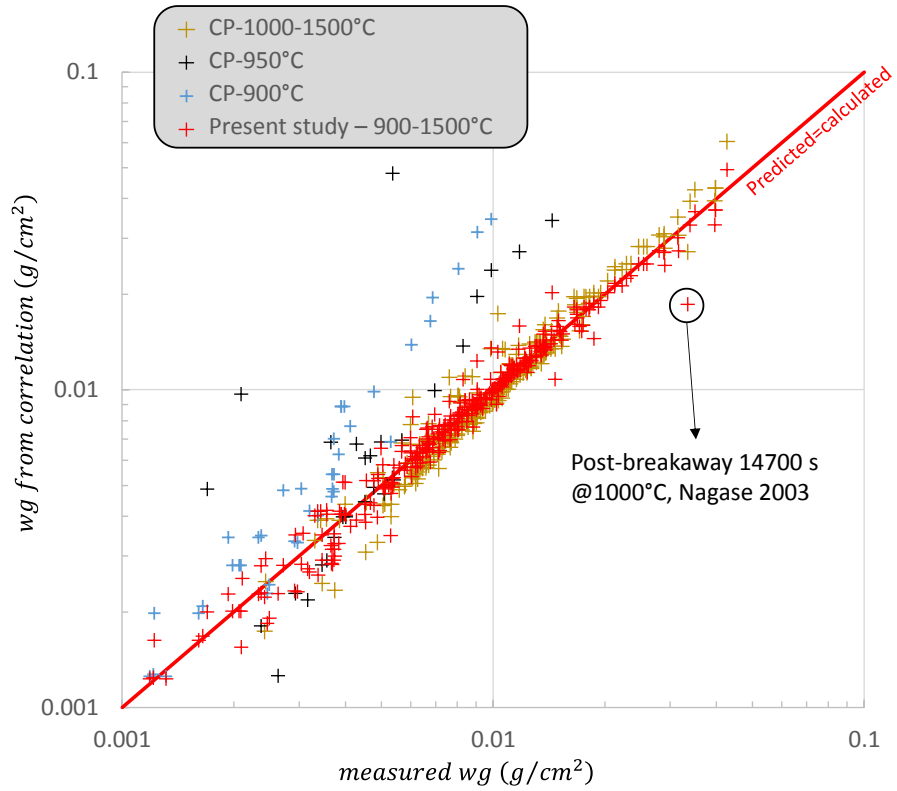

Figure 11: Accuracy of the present paper prediction and the Cathcart-Pawel correlation (its validity range being 1000-1500°C)

The standard deviation in each temperature category is assumed to follow a log-normal distribution:

$$wg = \overline{wg}.\, e^{\aleph(0,\sigma)} \qquad (14)$$

Temperature (°C)	900	950	1000	1100	1200	1300	1400	1500
Present study - σ	0.093	0.122	0.103	0.059	0.042	0.037	0.013	0.020
Cathcart-Pawel - σ	0.650*	0.663*	0.155	0.063	0.049	0.081	0.038	0.035

Table 5: Standard deviation, σ, of the log-normal variation of the estimated wg (*: out of correlation validity range).

It appears useful to describe a simple procedure facilitating the wg integration during a temperature transient. Equation 12 can be simplified into equation 1 type form $(wg)^{n(T)} = K(T)$. t and the time derivative form can straight forward be written as $\frac{d[(wg)^{n(T)}]}{dt} = K(T)$. Consequently, discretizing time and temperature into $\{t_i\}_{i=1,\dots,N}$ and $\{T_i\}_{i=1,\dots,N}$ and assuming negligible temperature change between two-time intervals, the weight-gain at t_{i+1} can be determined sequentially using its value at t_i:

$$wg_{i+1} = \left[wg_i{}^{n(T_{i+1})} + K(T_{i+1})t_{i+1} - K(T_i)t_i\right]^{\frac{1}{n(T_{i+1})}}$$

Nevertheless, a time sampling sensitivity analysis is recommended.

4 Discussion and conclusions

The present study has revisited the past and recent works addressing weight-gain kinetics for Zircaloy-4 tubes under steam environment at elevated temperature. A new method based on metallographic layer thickness measurements to evaluate local weight-gain has been proposed. It is validated by comparing weight-gain measurement to the calculated values on experiments performed at IRSN.

Two main aspects have not been analyzed in the present work: (1) the formation of α(O) inclusions in the ex-β central layer has not been considered; therefore, for long term exposure weight-gain are probably under-predicted, (2) the detailed distribution of oxygen within the oxide scale has not been considered. There is here a lack of knowledge, however it has a negligible impact on the evaluation of the weight-gain (because the gradient of oxygen concentration is small).

Simulation codes postulating oxygen transport by diffusion mechanism are expected to predict weight-gains following a parabolic increase with exposure duration assuming constant diffusivity values. Non parabolic trend prediction requires complex modeling refinement. Specifically, it is expected that stress and/or phase transformation influence the oxide crystallography across the zirconia layer which directly modifies the oxidation kinetics as suggested by Gosset [GOS15].

In the present study, a few simple assumptions facilitate the experimental data interpretation without any a priori assumptions on the oxygen transport mechanism in the oxide layer. This approach provides accurate weight-gain evaluations for isothermal oxidation conditions in the 900-1500°C range. On the contrary, for complex transients, oxidation simulation codes modelling the diffusions processes are necessary.

Modeling of the oxygen diffusion in a mixture of $\beta + \alpha(O)$ inclusions remains an axis of progress. This might help determining oxidation rate for very long exposures to steam at elevated temperature or in the lower range of the $\alpha+\beta$ domain.

To achieve progress in oxidation modeling there are several other aspects needing improvements. The main one is to determine the oxygen concentration profile across the oxide layer and model the key phenomena influencing this distribution. Tetragonal/monoclinic zirconia transformation facilitated by many possible phenomena such as grain size, local hydrostatic stress, sub-stoichiometry, temperature history might be of importance.

In the present study, the various steam oxidation experiments gathered are consistent with each other. An exception to this was an increase of the oxidation rate in the 950 and 1000°C experiments observed in Cathcart-Pawel and Leistikov experiments. This might result from a tin composition change between past and modern Zircaloy-4 or from a change in the alloy manufacturing route or surface finishing process. The high dispersion observed in the literature for the values of time to transition in this range of temperature is also probably linked to these changes.

Another outcome of the study is a single and simple correlation describing the weight-gain in a temperature range covering 900°C to 1500°C with a single correlation. Also, thanks to the large amount of gathered data (about 350 tests were analyzed), the data scatter was also characterized providing variation bands.

Finally, the main outcome of the present work is that, using the proposed method, a local weight-gain based on metallography can be determined after each complex experiment. This local approach helps to better understand complex experiments, verify the equivalent oxidation temperature conditions at a given section after an integral test and check the possible azimuthal temperature variations. The use of local weight-gain measurement can be used jointly with oxide layer thickness and oxygen stabilized α layer to better determine the local temperature and oxidation conditions.

Acknowledgement

The study relies on discussions that took place during several decades on Zircaloy-4 studies between different partners from CEA, FRAMATOME and EDF. They are thankfully acknowledged.

References

[ATI15] ATI – “Technical data Sheet – Zirconium Alloys” – Version 1 – Allegheny Technologies Incorporated – 1000 Six PPG Place, Pittsburg, PA 15222-5479 USA - (02/03/2015).

[BAK62] L. Baker, L. C. Just. “Studies of metal-Water reactions at high temperature – III Experimental and theoretical studies of the zirconium-water reaction”, ANL-6548. 1962.

[BAL76] R. G. Ballinger, W.G. Dobson, R.R. Biederman, "Oxidation reaction kinetics of Zircaloy-4 in an unlimited steam environment", Journal of Nuclear Materials, Volume 62, Issues 2–3, November 1976, Pages 213-220.

[BAR19] P. Barberis, R. Zino, "$M5_{FRAMATOME}$ cladding high temperature oxidation behavior during simulated LOCA transients", poster presented at the 19th International Symposium on Zirconium in the Nuclear Industry, Manchester, UK - May 19-23, 2019.

[BIL08] M. Billone, Y. Yan, T. Burtseva, R. Daum, "Cladding Embrittlement During Postulated Loss-of-Coolant Accidents", NUREG/CR-6967, 2008.

[BUD93] B. Budiansky, L. Truskinovsky, "On the mechanics of stress induced phase transformation in zirconia", Journal of Mechanics and Physics of Solids, vol. 41, pp. 1445-1459, 1993.

[BOU15] S. Boutin, S. Graff, "A new LOCA safety demonstration in France", Top Fuel meeting, 13-17 september 2015.

[BRA11] J.C. Brachet, D. Hamon, J.-L. Béchade, P. Forget, C. Toffolon-Masclet, C. Raepsaet, J.-P. Mardon, B. Sebbari, "Quantification of the chemical elements partitioning within pre-hydrided Zircaloy-4 after high temperature steam oxidation as a function of the final cooling scenario (LOCA conditions) and consequences on the (local) materials hardening", Proceedings of a Technical Meeting Held in Mito, Japan, 18–21 October 2011.

[CAB15] A. Cabrera, N. Waeckel, "A strength-based approach to define LOCA limits", Top Fuel meeting, 13-17 September 2015.

[CAT77] J.V. Cathcart. R.E. Pawel. R.A. McKee. R.E. Druschel. G.J. Yurek. J.J. Campbell. S.H. Jury. « Zirconium metal-water oxidation kinetics – IV Reaction rate studies », ORNL/NUREG/17, August 1977.

[CHU80] H. M. Chung, T. F. Kassner, "Embrittlement criteria for Zircaloy fuel cladding applicable to accident situations in light-water reactors: summary report", NUREG/CR-1344 – 1980.

[CHU79] H.M. Chung, T. F. Kassner, "Pseudobinary Zircaloy-Oxygen phase diagram", Journal of Nuclear Materials, vol. 84, pp. 327-339, 1979.

[DES21] J. Desquines, C. Duriez, S. Guilbert, T. Taurines, "High temperature oxidation and room temperature axial strength of pre-oxidized zircaloy-4 cladding after a simulated LOCA", Journal of Nuclear Materials 543 (2021).

[DOM76] R.F. Domagala, D.J. McPherson, « System zirconium-oxygen », Journal of Metals, vol. 6, n°2, pp. 238-246, 1954.

[DUR11] C. Duriez. S. Guilbert. A. Stern. C. Grandjean. L. Bělovský. J. Desquines. "Characterization of Oxygen Distribution in LOCA Situations", Journal of ASTM International, Vol. 8. No. 2 - Paper ID JAI103156, 2011.

[GEB61] E. Gebhardt, "Untersuchungen in system zirconium-sauerstoff – Teil 2 –Untersuchungen zur kinetic der reaction zwichen zirconium und sauerstoff. sowie über die constitution des systems zirconium-sauerstoff", Journal of Nuclear Materials Vol.4. n°3, (1961) pp. 255-268.

[GRA08] C. Grandjean, G. Hache, "A state of the art review of past programs devoted to fuel behavior under loss-of-coolant conditions – Part 3. Cladding oxidation, Resistance to quench and post-quench loads", IRSN Report DPAM/SEMCA 2008-093.

[GOS15] D. Gosset, M. Le Saux, "In-situ X-ray diffraction analysis of zirconia layer formed on zirconium alloys oxidized at high temperature", Journal of Nuclear Materials, vol. 458, pp. 245-252 (2015).

[GRO10] M. Grosse, “Comparison of the high temperature steam oxidation kinetics of advanced cladding materials”, Nuclear Technology, vol. 17, April 2020.

[GUE15] M. Guerain, C. Duriez, J. L. Grosseau-Poussard, and M. Mermoux, "Review of stress fields in Zirconium alloys corrosion scales," Corrosion Science, vol. 95, pp. 11-21, 2015.

[GUI10] S. Guilbert, C. Duriez, C. Grandjean, “Influence of a pre-oxide layer on oxygen diffusion on post-quench mechanical properties of Zircaloy-4 after steam oxidation at 900°C”, Proceedings of 2020 LWR Fuel Performance/Topfuel, Orlando, Florida, USA, September 26-29, 20210, paper 121.

[GUI16] S. Guilbert-Banti, P. Lacote, G. Taraud, P. Berger, J. Desquines, C. Duriez, « Influence of hydrogen on the oxygen solubility in Zircaloy-4”, Journal of Nuclear Materials 469 (2016) 228-236

[GUI16B] S. Guilbert, J. Desquines, “Fuel cladding post-quench LOCA embrittlement: mechanical test relevance”, Top Fuel 2016, Boise, ID, September 11-15, 2016.

[GUI19] R. Guillou, M. Le Saux, E. Rouesne, D. Hamon, C. Toffolon-Masclet, D. Menut, J. C. Brachet, J. L. Béchade, and D. Thiaudière, "In-situ time-resolved study of structural evolutions in a zirconium alloy during high temperature oxidation and cooling," Materials Characterization, vol. 158, p. 109971, 2019.

[GUI21] S. Guilbert-Banti, A. Viretto, J. Desquines, C. Duriez, « Effect of pre-oxide on Zircaloy-4 high temperature steam oxidation », Journal of Nuclear Materials, vol. 548, 2021.

[KAW78] S. Kawasaki, T. Furuta, M. Suzuki, «Oxidation of Zircaloy–4 under high temperature steam atmosphere and its effect on ductility of cladding», Journal of Nuclear Science and Technology, vol. 15, pp. 589-596, 1978.

[KIM21] D. Kim, H. Yook, K. Keum. Y. Lee, “TRANOX: Model for non-isothermal steam oxidation of Zircaloy cladding”, Journal of Nuclear Materials, Vol. 556, 2021.

[LEI83] S. Leistikov, G. Schantz, H. V. Berg, A. E. Aly, “Comprehensive presentation of extended Zircaloy-4 steam oxidation results 600-1600°C”. PCDE-NEA-CSNI/IAEA Specialists’ Meeting on Water Reactor Fuel Safety and Fission Products Release in Off-Normal and Accident Conditions, Riso National Laboratory (Denmark), 16-20 May 1983.

[LEI87] S. Leistikov, G. Schantz, « Oxidation kinetics and related phenomena of Zircaloy-4 fuel cladding exposed to high temperature steam and hydrogen-steam mixtures under PWR accident conditions ». Nuclear Engineering and Design, vol. 103, (1987), p.p. 65-84.

[LEM57] A. W. Lemmon. Jr. "Studies Relating to the Reaction Between Zirconium and Water at High Temperatures." BMI-1154, Battelle Memorial Institute, (Jan. 1957).

[LES11] M. Le Saux, J.C. Brachet, V. Vandenberghe, D. Gilbon, J.P. Mardon, B. Sebbari, “Influence of Pre-Transient Oxide on LOCA High Temperature Steam Oxidation and Post-Quench Mechanical Properties of Zircaloy-4 and M5™ cladding” - 2011 Water Reactor Fuel Performance Meeting – Chengdu, China, Sept. 11-14. 2011.

[MA08] X. Ma, C. Toffolon-Masclet, T. Guilbert. D. Hamon. J.-C. Brachet. « Oxidation kinetics and oxygen diffusion in low-tin Zircaloy-4 up to 1523 K”. Journal of Nuclear Materials 377 (2008) 359–369.

[MAT93] C.M. Allison, G.A. Berna, R. Chambers, E.W. Coryell, K.L. Davies, D.L. Hagrman, D.T. Hagrman, N.L. Hampton, J. K. Hohorst, R. E. Mason, M.L. McComas, K.A. McNeil, R.L. Miller, C.S.

Olsen, G.A. Reymann, L. J. Siefken, “SCAP/RELAP5/MOD3.1 Code Manual – Volum IV: MATPRO – A Library of Materials Properties for Light-Water-Reactor Accident Analysis”, NUREG/CR-6150, 1993.

[MAZ13] B. Mazères, C. Desgranges, C. Toffolon-Masclet, D. Monceau, "Contribution to Modeling of Hydrogen Effect on Oxygen Diffusion in Zy-4 Alloy During High Temperature Steam Oxidation", Oxidation of Metals, vol.79, issue (1-2). 2013.

[NAG03] F. Nagase, T. Otomo, H. Uetsuka, ”Oxidation Kinetics of Low-Sn Zircaloy-4 at the Temperature Range from 773 to 1.573 K”, Journal of NUCLEAR SCIENCE and TECHNOLOGY, Vol. 40, No. 4, p. 213–219 (April 2003).

[NAR20] T. Narukawa, M. Amaya, “Oxidation behavior of high-burnup advanced fuel cladding tubes in high-temperature steam”, Journal of Nuclear Science and Technology, 2019, Vol. 56, n°7, pp. 650-660.

[PER77] R.A. Perkins, “Oxygen diffusion in β-Zircaloy”, Journal of Nuclear Materials, vol.68 (1977), pp. 148-160.

[POR05] L. Portier, T. Bredel, J.-C. Brachet, V. Maillot, J.-P. Mardon, A. Lesbros, “Influence of Long Service Exposures on the Thermal-Mechanical Behavior of Zy-4 and M5™ Alloys in LOCA Conditions”. Journal of ASTM International, February 2005, Vol. 2, No. 2 - Paper ID JAI12468.

[RUH66] R. Ruh, H. J. Garret, “Nonstoichiometry of ZrO2 and its relation to tetragonal-cubic inversion in ZrO2”, Journal of the American Ceramic Society. 50. 1966. pp.257-261.

[SCH03] G. Schanz, “Recommendations and supporting information on the choice of zirconium oxidation model in severe accident”, FZKA- Report 6827 – 2003.

[TOR17] E. Torres, J. Desquines, S. Guilbert, P. Lacote, M.-C. Baietto, M. Coret, M. Blat, A. Ambard, « Oxygen segregation in pre-hydrided Zircaloy-4 cladding during a simulated LOCA transient”, EPJ Nuclear Science and Technology, vol. 3, issue 27, 2017.

[URB78] V.F. Urbanic, T.R. Heindrick, “High temperature oxidation of Zircaloy-2 and Zircaloy-4 in steam”, Journal of Nuclear Materials 75, issue 2, (1978) pp. 251-261.

[WAG33] C. Wagner, “Beitrag zur theorie des anlaufvorgangs”, Zeitschrift für Physikalische Chemie, vol. B 21, pp. 25-41, 1933.

[ZIN21] R. Zino, R. Chosson, M. Ollivier, E. Serris, L. Favergeon, "Parallel mechanism of growth of the oxide and α-Zr(O) layers on Zircaloy-4 oxidized in steam at high temperatures," Corrosion Science, vol. 179, 2021.